

**Stabilizing the interface of NASICON solid electrolyte
against Li metal with atomic layer deposition**

Yulong Liu, Qian Sun, Yang Zhao, Biqiong Wang, Payam Kaghazchi, Keegan Adair, Ruying Li, Cheng Zhang, Jingru Liu, Liang-Yin Kuo, Yongfeng Hu, Tsun-Kong Sham, Li Zhang, Rong Yang, Shigang Lu, Xiping Song, and Xueliang Sun

ACS Appl. Mater. Interfaces, **Just Accepted Manuscript** • DOI: 10.1021/acsami.8b06366 • Publication Date (Web): 24 Aug 2018

Downloaded from <http://pubs.acs.org> on August 30, 2018

Just Accepted

“Just Accepted” manuscripts have been peer-reviewed and accepted for publication. They are posted online prior to technical editing, formatting for publication and author proofing. The American Chemical Society provides “Just Accepted” as a service to the research community to expedite the dissemination of scientific material as soon as possible after acceptance. “Just Accepted” manuscripts appear in full in PDF format accompanied by an HTML abstract. “Just Accepted” manuscripts have been fully peer reviewed, but should not be considered the official version of record. They are citable by the Digital Object Identifier (DOI®). “Just Accepted” is an optional service offered to authors. Therefore, the “Just Accepted” Web site may not include all articles that will be published in the journal. After a manuscript is technically edited and formatted, it will be removed from the “Just Accepted” Web site and published as an ASAP article. Note that technical editing may introduce minor changes to the manuscript text and/or graphics which could affect content, and all legal disclaimers and ethical guidelines that apply to the journal pertain. ACS cannot be held responsible for errors or consequences arising from the use of information contained in these “Just Accepted” manuscripts.

Stabilizing the Interface of NASICON Solid Electrolyte against Li Metal with Atomic Layer Deposition

Yulong Liu^{†,†}, Qian Sun^{†,†}, Yang Zhao[†], Biqiong Wang[†], Payam Kaghazchi[‡], Keegan R. Adair[†], Ruying Li[†], Cheng Zhang[#], Jingru Liu[#], Liang-Yin Kuo[‡], Yongfeng Hu[§], Tsun-Kong Sham[⊥], Li Zhang^{//}, Rong Yang^{//}, Shigang Lu^{//}, Xiping Song^{#,*}, Xueliang Sun^{†,*}

[†]Department of Mechanical and Materials Engineering, Western University, London, Ontario, N6A 5B9, Canada

[‡]Physikalische und Theoretische Chemie, Freie Universitat Berlin, D-14195 Berlin, Germany.

[#]State Key Laboratory for Advance Metal and Materials, University of Science and Technology Beijing, Beijing 100083, China

[§]Canadian Light Source, Saskatoon S7N 2V3, Canada

[⊥]Department of Chemistry, Western University, London, Ontario, N6A 3K7, Canada.

^{//} China Automotive Battery Research Institute Co., Ltd, Beijing, 100088, China

† Equally contributed

* Corresponding author: xsun9@uwo.ca and xpsong@skl.ustb.edu.cn

ABSTRACT Solid-state batteries have been considered as one of the most promising next-generation energy storage systems due to their high safety and energy density. Solid-state electrolytes are the key component of the solid state battery, which exhibit high ionic conductivity, good chemical stability, and a wide electrochemical windows. LATP ($\text{Li}_{1.3}\text{Al}_{0.3}\text{Ti}_{1.7}(\text{PO}_4)_3$) solid electrolyte has been widely investigated for its high ionic conductivity. Nevertheless, the chemical instability of LATP against Li metal has hindered its application in solid-state batteries. Here, we propose that atomic layer deposition coating on LATP surfaces is able to stabilize the LATP/Li interface by reducing the side-reactions. In comparison with bare LATP, the Al_2O_3 coated LATP by atomic layer deposition exhibits a stable cycling behavior with smaller voltage hysteresis for 600 hours, as well as small resistance. More importantly, based on advanced characterizations such as HRTEM-EELS, the lithium penetration into the

LATP bulk and Ti^{4+} reduction are significantly limited. The results suggest that atomic layer deposition is very effective in improving solid state electrolyte/electrode interface stability.

KEYWORDS Solid state electrolyte, interface, ALD, Al_2O_3 , HRTEM

Introduction

Lithium ion batteries (LIBs) have been widely applied in portable electronics and electric vehicles (EVs). However, there are still some concerns over the safety issues of commercial LIBs because of the use of flammable liquid electrolytes (LEs).^{1, 2, 3} Furthermore, the energy density of LE LIBs using current cathode and anode technology will reach its maximum limitation in the near future. Therefore, it is necessary to find alternative energy storage systems with higher energy density, such as Li metal batteries.^{4, 5, 6} Unfortunately, Li metal is unstable in LEs due to severe side reactions like electrolyte decomposition, which leads to gassing problems after many cycles. Moreover, dangerous Li dendrites are easily formed in batteries containing LEs, which leads to short circuits and thermal runaway.^{7, 8, 9} To solve these obstacles, solid state electrolytes (SSEs) are introduced into lithium batteries. They possess the merits of non-flammability, good stability and low degradation rate, enabling the fabrication of high-safety and high-energy-density solid state lithium ion batteries (SSLIBs).^{2, 6, 10, 11, 12}

The SSE plays a critical role in achieving high-energy-density SSLIBs in terms of electrochemical performance. SSEs have been widely developed over the past decades, including LISICON oxides,¹³ NASICON oxides,¹⁴ perovskite-type oxides,¹⁵ garnet-type oxides,¹⁶ and sulfide glass/glass ceramic/crystalline electrolytes.¹⁷ Additionally, some of them have achieved very high ionic conductivities at room temperature (close to 1 mS cm^{-1}), which is comparable to liquid electrolytes.¹⁸ Among these potential SSEs, NASICON-type electrolyte LATP ($\text{Li}_{1.3}\text{Al}_{0.3}\text{Ti}_{1.7}(\text{PO}_4)_3$) has received much attention after its initial development in the 1990s by Anno et al., and is capable of showing an ionic conductivity of 0.1 mS cm^{-1} at room temperature due to the doping of Al in the lattice.¹⁹ The LATP solid electrolyte films had already been used and exhibited excellent performance in Li- O_2 and Li sulfur hybrid electrolyte based batteries.^{4, 20, 21, 22, 23} Moreover, all SSLIBs were fabricated using LATP electrolyte and thin film cathode LiCoO_2 , which showed a good electrochemical performance at room temperature.^{24, 25} Employing a spark plasma sintering technique, Aboulaich et al. fabricated an all inorganic solid state battery based on $\text{Li}_{1.5}\text{Al}_{0.5}\text{Ge}_{1.5}(\text{PO}_4)_3$ (LAGP) electrolyte, which could be comparable to

1
2
3 the cycle performance of LE based battery.²⁶ Unfortunately, the use of Li metal as an anode is
4 still hindered due to the side reaction between LATP with Li. For example, the Ti^{4+} in LATP was
5 easily reduced by Li metal into Ti^{3+} , forming some interphases at the LATP/Li interface.²⁷ In a
6 recent study done by Janek et al., a mixed (ionic/electronic) conducting interphase (MCI) was
7 observed at the LAT(Ge)P/Li interface, which functioned similar to the solid electrolyte
8 interphase (SEI) layer formed in batteries with LE.²⁸
9

10 To improve the stability of LATP against Li metal, intermediate layers such as polymer
11 electrolytes were utilized at the LATP/Li interface.^{29, 30} The side-reactions were partially
12 mitigated by the chemical stability of the polymer interlayer, however, two additional interfaces
13 (LATP/polymer, Li/polymer) were introduced which might have a negative effect on
14 performance.³¹ For example, it was reported that the polymer electrolytes (PEO based) were
15 easily reduced by Li metal, and there was a risk of the formation of lithium dendrite at
16 Li/polymer interface.^{32, 33, 34} LiPON thin film electrolyte, synthesized by sputtering, has been
17 proven to be stable against Li metal in thin film solid state batteries.³⁵ Therefore, it was proposed
18 that a thin film of LiPON can act as a barrier on the LATP surface to improve stability. The
19 results showed that this interlayer was effective in reducing the side-reaction between LATP and
20 Li.^{36, 37} Recently, there has been an emerging interest in the protection of Li metal with surface
21 coatings in LE LIBs.^{38, 39} An ultrathin protection layer on Li metal could greatly improve the
22 performance of Li stripping/plating in LE-based batteries.³⁹ Atomic layer deposition (ALD) is a
23 unique deposition method that can realize excellent coverage and conformal depositions with
24 precise control over film thickness at the atomic level due to its self-limiting nature.⁴⁰ Recently,
25 our group has demonstrated that ALD coatings on the surface of Li metal could prevent the
26 direct contact of liquid electrolyte with electrode, thus enhancing stability and performance of
27 LIBs.⁴¹ In a paper published by Hu et al., it was shown that introducing an ultrathin Al_2O_3 *via*
28 ALD on garnet electrolyte ($Li_7La_3Zr_2O_{12}$) dramatically increased the wetting and chemical
29 stability against Li metal after forming a Li-Al-O intermediate layer.⁴² It is therefore assumed
30 that ALD coating on LATP can be an effective method in stabilizing the LATP/Li interface. The
31 ALD coating can not only avoid the direct contact of LATP with Li metal, but also form an
32 intermediate layer at the interface that is beneficial to Li-ion transport. In order to understand the
33 influence of interlayer ionic conductivity on the stability of LATP/Li interface, both Li-ion
34 conducting Li_3PO_4 and non-conducting Al_2O_3 interlayers are studied in our design.
35
36
37
38
39
40
41
42
43
44
45
46
47
48
49
50
51
52
53
54
55
56
57
58
59
60

1
2
3 In this paper, we demonstrate the successful application of the ALD Al_2O_3 coating on LATP
4 electrolyte to realize a highly stable LATP/Li metal interface. In addition, we have proved that
5 Al_2O_3 coated LATP shows a better stability than the bare and Li_3PO_4 coated LATP in the long-
6 term cycle tests. Through detailed characterizations at the interface, we ascribe the effective
7 protection of the LATP electrolyte to the dense and conformal ALD Al_2O_3 coating which acts as
8 a physical barrier and enables the formation of a Li-Al-O conducting layer after cycling.
9

14 Results and Discussion

16 NASICON type electrolytes (LATP) were prepared by a wet chemical method, and the as-
17 sintered pellets showed an ionic conductivity of 0.15 mS cm^{-1} at room temperature with an
18 activation energy of 0.3 eV (**Figure S1**), which was available for application in all solid state
19 batteries. The stability of the solid state electrolyte against Li metal was then evaluated by
20 Li/LATP/Li symmetrical cells, which were cycled at 0.01 mA cm^{-2} with limited capacity of 0.01
21 mA h cm^{-2} (each cycle takes 2 h). The Galvano-static cycle performance of the symmetrical cells
22 are presented in the **Figure 1**. It is seen that the pristine LATP cell shows a relatively low over
23 potential of 0.1 V at the first cycle, which indicates that the LATP and Li interface has good
24 contact. However, the over potential is progressively increased during the following cycles
25 (**Figure 1a**). It increase from 0.1 V to 3.5 V after 300 cycles (600 h), as shown in **Figure 1b**. In
26 a previous study, the Al_2O_3 layer by ALD was proven to act as a very robust and stable interlayer
27 in protecting Li metal in LE *via* limiting the side-reactions.³⁹ Based on calculation, the interlayer
28 inserted at the Li metal/electrolyte interface is about 10-20 nm in thickness.^{43, 44} Therefore, 15
29 nm thick of Al_2O_3 (about 150 cycles ALD) was coated on the surface of LATP solid electrolyte
30 by ALD to improve the stability of LATP against Li metal. As shown in **Figure 1c**, the Al_2O_3
31 coated LATP electrolyte (LATP@150 Al_2O_3), shows a different cycling behavior compared to
32 that of the bare LATP. A large over potential of 10 V is obtained in the first cycle, however, it
33 quickly decreases to 0.9 V after 100 cycles. More importantly, the over potential is stabilized at
34 this level with negligible change even after 300 cycles (600 h) (**Figure 1d**). The higher voltage
35 of LATP@150 Al_2O_3 in the first cycle is attributed to the insulating nature of the Al_2O_3 layer,
36 which has been reported on other Al_2O_3 coated materials.⁴⁵ After the initial Al_2O_3 layer lithiation
37 process, the potential gradually decreases and the ion-conducting layer remains stable during the
38 following cycles, as seen in **Figure 1c**. In addition to the non-conductive Al_2O_3 layer, another
39
40
41
42
43
44
45
46
47
48
49
50
51
52
53
54
55
56
57
58
59
60

1
2
3 lithium conducting Li_3PO_4 interlayer coating was deposited on LAMP electrolyte to understand
4 the lithium transporting properties and its influence on the interface. An ALD coating of 175
5 cycles of Li_3PO_4 (about 15 nm, similar to the Al_2O_3 layer) was deposited on LAMP. The over
6 potential of LAMP@175 Li_3PO_4 electrolyte against Li metal is 0.3 V in the first cycle, which is
7 0.2 V higher than the bare LAMP electrolyte. The small increase of potential in
8 LAMP@175 Li_3PO_4 is ascribed to the relatively low ionic conductivity of the Li_3PO_4 electrolyte
9 compared to that of LAMP.⁴⁶ The potential remains stable at this level for the following 25 cycles
10 with small changes. Nevertheless, the over potential of the LAMP@175 $\text{Li}_3\text{PO}_4/\text{Li}$ starts to grow
11 and rise to 0.8 V, 2.4 V and 4 V at the 100th, 200th and 300th cycle, respectively, which may be
12 due to the degradation of LAMP@175 Li_3PO_4 during repeated lithium stripping/plating (**Figure**
13 **1e, 1f**).

14
15 To further support the observations, we conducted the electrochemical impedance spectroscopy
16 (EIS) on the symmetrical cells before and after 300 cycles of Li plating and stripping. As shown
17 in **Figure S2a**, the impedance of bare LAMP increases from 6 K ohm to 400 K ohm after 300
18 cycles, which is consistent with the increase of voltage hysteresis. It is suggested that a high-
19 resistance interphase is formed at the interface of LAMP/Li, and the resistant layer thickness is
20 increased during cycling. Although the impedance of LAMP@150 Al_2O_3 cell is very large (8000
21 K ohm) because of the insulating Al_2O_3 coating on LAMP, the impedance decreases drastically to
22 only 150 K ohm after 300 cycles, which indicate the formation of an ion-conducting layer
23 between LAMP@150 Al_2O_3 and Li metal (**Figure S2b, Table S1**). LAMP@175 Li_3PO_4 presents
24 a small increment of impedance compared to bare LAMP before cycle, 6 K ohm to 10 K ohm.
25 The ALD coated Li_3PO_4 is an ionic conducting layer, but the conductivity of the Li_3PO_4 coating
26 is much lower than the bulk LAMP.⁴⁶ The impedance of the LAMP@175 Li_3PO_4 increases to 350
27 K ohm after 300 cycles, as shown in **Figure S2c**. When comparing the impedance of the three
28 cells after cycling, it can be concluded that the smaller impedance obtained in LAMP@ Al_2O_3 cell
29 is in good agreement with the long term cycling tests. Due to the high impedance at room
30 temperature, the interfacial contact is so poor so that a large over-potential is obtained.
31 Additionally, we conducted another experiment at evaluated temperature, it shows the same
32 trend as room temperature cell with a much low over-potential in **Figure S2d**. Therefore, we
33 propose that the lithiation mechanism of different ALD coating is varied, as shown in **Figure S3**.

1
2
3 Different cycles of ALD Al_2O_3 (25, 50, 100, 150, 200, 250 cycles) were coated on LATP in order
4 to investigate the ALD layer thickness effect on the lithium plating/stripping performance. As
5 shown in **Figure S4 a, b**, both $\text{LATP}@250\text{Al}_2\text{O}_3$ and $\text{LATP}@200\text{Al}_2\text{O}_3$ are thick enough to
6 show a stable interface during lithium plating/stripping. However, the voltage over-potential of
7 $\text{LATP}@250\text{Al}_2\text{O}_3$ and $\text{LATP}@200\text{Al}_2\text{O}_3$ are significantly higher (5 V and 2 V, respectively)
8 than that of $\text{LATP}@150\text{Al}_2\text{O}_3$ (0.9 V) (**Figure S5 a, b**). If we reduce the Al_2O_3 thickness to 100
9 cycles ALD, the voltage hysteresis drops to a 1 V in the beginning but slightly increases after
10 200 cycles, as shown in **Figure S4d**. Upon closer inspections, we can see the overpotential of the
11 $\text{LATP}@100\text{Al}_2\text{O}_3$ at the 1st, 100th, 200th and 300th are 8V, 0.8 V, 1.2 V and 1.5 V, respectively
12 (**Figure S5d**). This suggests that the 100 cycles of Al_2O_3 on LATP is not thick enough to
13 achieve a stable LATP/Li interface. When two thinner Al_2O_3 layers are applied on LATP, the
14 overpotential at the first cycle of $\text{LATP}@50\text{Al}_2\text{O}_3$ and $\text{LATP}@25\text{Al}_2\text{O}_3$ are reduced to as low as
15 6 V and 2 V, respectively (**Figure S5e, f**). Additionally, they only show an overpotential of 0.8 V
16 and 1 V after 100 cycles, respectively, after lithium penetration into the Al_2O_3 interlayer.
17 Unfortunately, the overpotential of $\text{LATP}@25\text{Al}_2\text{O}_3$ and $\text{LATP}@50\text{Al}_2\text{O}_3$ increases to 2.25 V
18 and 2 V after 300 cycles, respectively, indicating the instability of the LATP/Li interface.
19 Therefore, it is concluded that the $\text{LATP}@150\text{Al}_2\text{O}_3$ is the best among the six thicknesses
20 studied for stabilizing the LATP/Li interface in terms of cycle time and voltage hysteresis. As
21 shown in **Figure S6a**, the impedance spectra of $\text{LATP}@50\text{Al}_2\text{O}_3$, $\text{LATP}@100\text{Al}_2\text{O}_3$,
22 $\text{LATP}@150\text{Al}_2\text{O}_3$, and $\text{LATP}@200\text{Al}_2\text{O}_3$ are recorded before and after 300 cycle's lithium
23 plating/stripping. Before cycling, all the Al_2O_3 coated LATP electrolytes show large impedance
24 because of the insulating nature of Al_2O_3 film. The value of the impedance increases from 1500
25 K ohm to 10000 K ohm, as the thickness of Al_2O_3 film increases from 50 to 200 ALD cycles
26 (**Table S2**). After 300 cycles of lithium plating/stripping, the impedance among all four cells
27 drops quickly, which is in consistent with the changes in overpotential (**Figure S6b**). The drop in
28 impedance may indicate that an ion-conductive interphase was formed at the interface of Al_2O_3
29 coated LATP/Li. More importantly, we can see that the $\text{LATP}@150\text{Al}_2\text{O}_3$ shows the lowest
30 impedance out of all the coated LATP cells (**Table S2**), which further supports that 150 Al_2O_3
31 cycle is optimal for ALD-coated LATP.
32
33

34 In order to understand the ALD coating-layer position effect at the LATP/Li interface, the 75
35 cycles Al_2O_3 on Li and 75 cycles Al_2O_3 on LATP as a bi-layer protection coating was designed.
36
37
38
39
40
41
42
43
44
45
46
47
48
49
50
51
52
53

1
2
3 As shown in **Figure S7a**, the bi-layer cell shows a stable performance in the long term cycling.
4 However, the overpotential is much higher (5.5 V) than the LATP@150Al₂O₃ (0.9 V). This
5 result suggests that the side-reaction at the LATP/Li interface is limited by the bi-layer coating
6 but the lithium transport paths are partially blocked at interface. In addition to the bi-layer
7 coating, a previous study suggested that Al₂O₃ ALD coating on Li metal also exhibited stable
8 performance in liquid electrolyte.³⁹ Therefore, only 75 cycles the Al₂O₃ ALD coating on Li metal
9 was investigated, as presented in **Figure S7b**. The single coating on Li metal performs worse
10 than the bi-layer and single coatings on LATP with an increased over potential during cycling,
11 indicating the formation of an unstable LATP/Li interface. Therefore, it has been proven that the
12 coating of Al₂O₃ on the LATP surface is more effective than coating on the Li metal surface, and
13 with better performance than coatings on both the LATP and Li metal surfaces.
14
15
16
17
18
19
20
21
22

23 To explore the effect of the ALD coating layer on the LATP after the lithium stripping/plating
24 process, the cross-section of LATP pellets after 100 cycles were examined by scanning electron
25 microscope (SEM). By comparing the secondary electrons images of bare LATP,
26 LATP@175Li₃PO₄ and LATP@150Al₂O₃ (**Figure S8**), it is difficult to observe any significant
27 difference in morphology. Therefore, backscattering electron images (BSE) were utilized due to
28 their increased sensitivity to the chemical composition. As shown in **Figure 2a**, we can see that
29 the surface of the LATP pellet shows regions of darker color compared to the white bulk LATP,
30 which is an indication of lithium penetration into the LATP electrolytes and LATP electrolyte is
31 reduced by Li.²⁸ The reduction depths of bare LATP, LATP@175Li₃PO₄ and LATP@150Al₂O₃
32 are all in the range of micro level as shown in the BSE images, however more detailed
33 structure/chemical information of cycled LATP should be obtained by other characterization
34 techniques. The GIXRD pattern of LATP@175Li₃PO₄ and LATP@150Al₂O₃ were conducted
35 before and after contact with Li metal (**Figure S9**). Unfortunately, no changes are observed. In
36 addition, we did the XRD on the three cycled LATP solid electrolytes. The lithiated phase of
37 NASICON type structure, Li₃Al_{0.3}Ti_{1.7}(PO₄)₃ phase is observed in the solid electrolytes. (**Figure**
38 **S10**)
39
40
41
42
43
44
45
46
47
48
49
50

51 In order to obtain evidence of the reduction of Ti element in the LATP electrolyte, we conduct a
52 chemical composition test on the LATP samples before and after cycling with high energy X-ray
53 photoelectron spectroscopy (HE-XPS) in Canadian Light Source at the SXRMB beamline. The
54
55
56
57
58
59
60

1
2
3 HE-XPS is able to provide chemical information with controlled probing depth that is not limited
4 to the surface but extended beyond 10 nm in bulk samples, in comparison to laboratory XPS.^{47, 48}
5 For example, we choose three excitation energies of 3000 eV, 4500 eV and 6000 eV, which are
6 able to detect different depth for Ti 2p.^{49, 50} The valence states of Ti in bare LATP before and
7 after cycling are evaluated at three different excitation photon energies (3 keV, 4.5 keV and 6
8 keV), and the results are illustrated in **Figure 2 b**. The LATP sample prior to cycling show
9 mainly Ti⁴⁺ (459.3 eV) at all probing depths with a minor fraction of Ti³⁺ (~458.1 eV) peak
10 appearing at photon energies of 3 and 4.5 keV (**Figure 2b**). This is because of the slight
11 reduction of LATP in the preparation and storage process, which has also been observed by a
12 previous study.²⁸ After lithium stripping /plating, more Ti⁴⁺ in the near surface region of bare
13 LATP is reduced to Ti³⁺ as shown in **Figure 2b**. Furthermore, the reduction to the Ti³⁺ state is
14 observed at all probed depths with the fraction at the photon energy of 6 keV being still 14%
15 after cycling (**Table S3**). For the LATP@175Li₃PO₄ pellet after cycling, the Ti³⁺ primarily
16 appears only at the photon energy of 3 KeV (**Figure 2b and Table S3**). It is difficult to resolve
17 the Ti³⁺ fraction in the deeper depth, which suggests that the Ti reduction is prevented after the
18 application of a Li₃PO₄ coating on LATP. The fraction of Ti³⁺ in the LATP@150Al₂O₃ after
19 cycling will be investigated by the EELS line scan in the following section in detail to
20 understand the protection behavior of the Al₂O₃ layer.
21
22
23
24
25
26
27
28
29
30
31
32
33
34

35 The three solid electrolyte pellets after cycling were cut with a focused ion beam (FIB), and the
36 LATP/Li interfaces were characterized with high resolution transmission electron microscope
37 (HR-TEM) in order to get clear structural and chemical information about the LATP surface and
38 LATP/Li interface. As illustrated in **Figure 3**, we present the morphology and elemental
39 distribution of bare LATP, LATP@175Li₃PO₄ and LATP@150Al₂O₃ against Li metal at the
40 interface. As seen from the EDS mapping of bare LATP after 100 cycles in **Figure 3a**, the
41 surface of LATP is very rough and porous, and some dendrite structures are observed. This
42 indicates that the Li has penetrated into the bulk of LATP electrolyte and some Li dendrites are
43 formed near the surface. Furthermore, the Li diffused into the LATP electrolyte for several
44 hundred nanometers and accumulated between the grains as seen by the bright and dark field (BF
45 and DF) images (**Figure 3a**, TEM images). On the contrary, no rough surface has been observed
46 for LATP@175Li₃PO₄ after cycling (**Figure 3c**), which suggests the Li₃PO₄ coating is effective
47 in preventing Li penetration and dendrite formation. It is noteworthy that it is difficult to
48
49
50
51
52
53
54
55
56
57
58
59
60

1
2
3 distinguish the Li_3PO_4 layer by the EDS because the bulk solid electrolyte also contains
4 phosphate. Although the $\text{LATP}@175\text{Li}_3\text{PO}_4$ shows a flat surface after cycling, the BF and DF
5 TEM images in **Figure 3c** show some cracks formed in bulk LATP, which may be the reason for
6 LATP degradation after longer cycles. This is also related the mechanical properties of the
7 coating layer. According to previous study, the cracks are due to the migration of Li-ion into the
8 grain boundary during lithium stripping and plating.⁵¹ In **Figure 3b**, an obvious layer of Al_2O_3 is
9 observed at the interface of $\text{LATP}@150\text{Al}_2\text{O}_3/\text{Li}$ even after long cycles, which suggests that the
10 coating is very robust and adheres well to the surface. Similar to the Li_3PO_4 coated sample, no
11 rough surface and pores could be detected at the $\text{LATP}@150\text{Al}_2\text{O}_3$ interface, suggesting good
12 protection of Al_2O_3 . Moreover, we do not see lithium diffusion into the LATP electrolyte and no
13 crack is formed in the bulk LATP according to the DF and BF images (**Figure 3b**, TEM images).
14 This exhibits that the $\text{LATP}@150\text{Al}_2\text{O}_3/\text{Li}$ interface is free of Li dendrite and cracks, providing
15 evidence and reasoning for the stable cycle performance of $\text{LATP}@150\text{Al}_2\text{O}_3$ compared to the
16 bare LATP/Li and $\text{LATP}@175\text{Li}_3\text{PO}_4/\text{Li}$. To verify our assumption, another Li conductor layer
17 LiTaO_3 was coated on LATP, it showed that lithium ions could still penetrate the coating layer
18 (**Figure S11**).

19
20
21
22
23
24
25
26
27
28
29
30
31 As is well known, the Ti reduction phenomenon is very critical for the LATP electrolyte in
32 coupling with Li metal. The above XPS result has provided useful information about the Ti
33 reduction situation at a macroscopic level.³⁶ With the help of electron energy loss spectroscopy
34 (EELS) detector in HR-TEM, we are able to obtain the chemical information of elements at the
35 nano-scale level. The EELS mapping of the bare LATP after 100 cycles and Ti valence state
36 depth profiles are presented in **Figures 4a and 4b**. It is seen from the Li and Ti line profiles that
37 there is a distinct line between LATP and Li, while there is a clear sharp change in Ti and Li
38 elemental intensities. It is the same situation in the EELS mapping, in which Ti and Li are
39 enriched in different regions. However, upon closer inspection some Li element is found to
40 penetrate into the LATP and reside at the grain boundaries, as circled in the EELS mapping in
41 **Figure 4a**. By focusing on the Ti, an EELS line scan of Ti $L_{3,2}$ edge from LATP/Li interface to
42 LATP bulk is recorded in **Figure 4b**. The Ti^{3+} L_3 main peak (~ 464.8 eV) is dominant from the
43 interface to a depth of 24 nm in the energy loss spectra. Beyond that, two extra shoulder peaks
44 appear and the L_3 main peak position shifts to a relatively higher energy of ~ 465.8 eV, which is
45 an indication of Ti^{4+} signal. The Ti^{4+} signal becomes stronger while the Ti^{3+} decreases along the
46
47
48
49
50
51
52
53
54
55
56
57
58
59
60

1
2
3 penetration depth line, that is, Ti^{4+} becomes dominant from 28 nm at the interface to bulk
4 LATP.^{52, 53} Unlike the bare LATP, the EELS mapping on $\text{LATP}@150\text{Al}_2\text{O}_3$ after 100 cycles
5 shows the formation of stable interface on the LATP pellet (**Figure 4c**). Similar to the EDS map,
6 a layer of Al_2O_3 is clearly found, and no Li penetration is detected at the interface region.
7 Interestingly, from the composite map of Li-Al-O, it is believed that a lithium containing layer is
8 formed on the LATP surface after the lithium stripping and plating process, which could be the
9 origin of the voltage drop and impedance decrease. In the Ti line scan result as illustrated in
10 **Figure 4d**, the Ti^{3+} dominant depth decreased from 24 nm in bare LATP to 16 nm in
11 $\text{LATP}@150\text{Al}_2\text{O}_3$, suggesting that the Ti reduction is prevented (or reduced?) in LATP
12 electrolyte. It is also noteworthy to mention that the Ti line scan is drawn along the region where
13 Li is rich (refer to the EELS map, where Ti line scan is crossing in the green Li rich region). If
14 we consider the average distribution, the reduction depth of Ti should be smaller on average. The
15 Ti EELS results also agree well with the macroscopic XPS results, providing evidence that the
16 Al_2O_3 coating is effective in stabilizing the LATP/Li interface. Recently, it is thought that
17 morphological changes are challenging to compensate by cell design and some mechanical
18 formation step is needed. Therefore, soft interlayer is needed to accommodate the volume change
19 at interface in the future.^{54,55}

20
21
22
23
24
25
26
27
28
29
30
31
32
33 The detailed stabilization mechanism of the stabilization of the LATP/Li interface by ALD is
34 presented in **Figure 5a**, and illustrates that the Al_2O_3 coating functions as both a physical barrier
35 and a shield to protect the Ti in LATP from further reduction. In the bare LATP, Li dendrites are
36 formed and Ti reduction progressively penetrates into bulk region. To validate our model for the
37 LATP structure we have simulated its XRD pattern. The calculated XRD pattern is in good
38 agreement with our experimental results (**Figure S12**). To study the stability of electrolyte and
39 coating layer in contact with a Li metal, we have calculated absorption energies of a single Li
40 atom in LATP and $\alpha\text{-Al}_2\text{O}_3$, respectively. Our DFT calculations show that the absorption energy
41 of a single Li inside LATP is a high negative value of -2.88 eV, which can indicate instability of
42 LATP with respect to Li metal. However, the absorption energy of a single Li in $\alpha\text{-Al}_2\text{O}_3$
43 possesses a largely positive value of +3.17 eV, which can provide evidence for the high stability
44 of this coating material against Li metal, as shown in **Figure 5b**. Moreover, we have studied the
45 possibility of $\text{Al} \leftrightarrow \text{Ti}$ interchange between LATP and $\alpha\text{-Al}_2\text{O}_3$ following the procedure
46
47
48
49
50
51
52
53
54
55
56
57
58
59
60

1
2
3 presented in **Figure 5c**. It is found that the interchange is unfavorable from a thermodynamic
4 point of view since it requires 3.22 eV energy.
5
6

7
8 In this work, we have successfully synthesized a LATP electrolyte with an ionic
9 conductivity of 0.15 mS cm⁻¹ at room temperature. Through modification of the LATP surface
10 by ALD Al₂O₃ coating, we obtain a highly stable LATP/Li interface with a cycle time of 600 hrs.
11 The LATP@150Al₂O₃ shows much better performance than the bare LATP and LATP@175
12 Li₃PO₄, with an overpotential of only 0.9 V after 300 cycles (LATP, 3.5 V and LATP@175
13 Li₃PO₄, 3.8 V). Based on the lithium stripping/plating test, the thickness of the protection layer
14 has been optimized with 150 cycles of Al₂O₃ on LATP yielding the most stable performance and
15 lowest overpotential. Furthermore, it is proved that coating on the LATP surface is more
16 effective than coating directly on Li metal. With the comprehensive characterizations, we find
17 that the both Li penetration and Ti reduction are prevented by the dense Al₂O₃ coating, which
18 enables the realization of a stable interface at LATP/Li. In addition, the Al₂O₃ coating is
19 transformed to a Li-Al-O conducting layer, which acts as the lithium transport pathway at the
20 LATP/Li interface and largely reduces the interface resistance.
21
22
23
24
25
26
27
28
29
30
31
32
33
34

35 ASSOCIATED CONTENT

36
37
38 **Supporting Information.** Experimental details, additional physical and electrochemical
39 characterization. This material is available free of charge via the Internet at <http://pubs.acs.org>.
40
41
42
43

44 AUTHOR INFORMATION

45 46 **Corresponding Author**

47
48
49 * E-mail: xsun9@uwo.ca and xpsong@skl.ustb.edu.cn
50
51

52 53 **Notes**

54
55 The authors declare no competing financial interests.
56
57
58
59
60

ACKNOWLEDGMENT

This research was supported by the China Automotive Battery Research Institute, Beijing, Nature Science and Engineering Research Council of Canada (NSERC), the Canada Research Chair Program (CRC), Canada Foundation for Innovation (CFI), the Canadian Light Sources (CLS), and the University of Western Ontario. Q.S and B.W. acknowledge the receipt of from the CLS Post-Doctoral student Travel Support program. J.Liu, C.Zhang and X.Song acknowledge the support of State Key Lab of Advanced Metals and Materials, University of Science and Technology Beijing, Beijing, China.

REFERENCES

- (1) Inoue T.; Mukai K. Are All-Solid-State Lithium-Ion Batteries Really Safe?-Verification by Differential Scanning Calorimetry with an All-Inclusive Microcell. *ACS Appl. Mater. Interfaces* **2017**, *9*, 1507-1515.
- (2) Chen R. J.; Qu W. J.; Guo X.; Li L.; Wu F. The Pursuit of Solid-State Electrolytes for Lithium Batteries: From Comprehensive Insight to Emerging Horizons. *Mater. Horiz.* **2016**, *3*, 487-516.
- (3) Kalhoff J.; Eshetu G. G.; Bresser D.; Passerini S. Safer Electrolytes for Lithium-Ion Batteries: State of the Art and Perspectives. *Chemsuschem* **2015**, *8*, 2154-2175.
- (4) McCloskey B. D. Attainable Gravimetric and Volumetric Energy Density of Li-S and Li Ion Battery Cells with Solid Separator-Protected Li Metal Anodes. *J. Phys. Chem. Lett.* **2015**, *6*, 4581-4588.
- (5) Zhang H.; Li C.; Piszcz M.; Coya E.; Rojo T.; Rodriguez-Martinez L. M.; Armand M.; Zhou Z. Single Lithium-Ion Conducting Solid Polymer Electrolytes: Advances and Perspectives. *Chem. Soc. Rev.* **2017**, *46*, 797-815.
- (6) Sun C. W.; Liu J.; Gong Y. D.; Wilkinson D. P.; Zhang J. J. Recent Advances in All-Solid-State Rechargeable Lithium Batteries. *Nano Energy* **2017**, *33*, 363-386.

- 1
2
3 (7) Hausbrand R.; Cherkashinin G.; Ehrenberg H.; Gröting M.; Albe K.; Hess C.; Jaegermann W. Fundamental Degradation Mechanisms of Layered Oxide Li-Ion Battery Cathode Materials: Methodology, Insights and Novel Approaches. *Mater. Sci. Eng. B* **2015**, *192*, 3-25.
- 4
5
6
7
8 (8) Gauthier M.; Carney T. J.; Grimaud A.; Giordano L.; Pour N.; Chang H. H.; Fenning D. P.; Lux S. F.; Paschos O.; Bauer C.; Maglia F.; Lupart S.; Lamp P.; Shao-Horn Y. Electrode-Electrolyte Interface in Li-Ion Batteries: Current Understanding and New Insights. *J. Phys. Chem. Lett.* **2015**, *6*, 4653-4672.
- 9
10
11
12
13
14 (9) Xu K. Electrolytes and Interphases in Li-Ion Batteries and Beyond. *Chem. Rev.* **2014**, *114*, 11503-11618.
- 15
16
17
18 (10) Quartarone E.; Mustarelli P. Electrolytes for Solid-State Lithium Rechargeable Batteries: Recent Advances and Perspectives. *Chem. Soc. Rev.* **2011**, *40*, 2525-2540.
- 19
20
21
22 (11) Thangadurai V.; Narayanan S.; Pinzaru D. Garnet-Type Solid-State Fast Li Ion Conductors for Li Batteries: Critical Review. *Chem. Soc. Rev.* **2014**, *43*, 4714-4727.
- 23
24
25
26 (12) Bachman J. C.; Muy S.; Grimaud A.; Chang H.-H.; Pour N.; Lux S. F.; Paschos O.; Maglia F.; Lupart S.; Lamp P.; Giordano L.; Shao-Horn Y. Inorganic Solid-State Electrolytes for Lithium Batteries: Mechanisms and Properties Governing Ion Conduction. *Chem. Rev.* **2016**, *116*, 140-162.
- 27
28
29
30 (13) Alpen U. v.; Bell M. F.; Wichelhaus W.; Cheung K. Y.; Dudley G. J. Ionic Conductivity of $\text{Li}_{14}\text{Zn}(\text{GeO}_{44})$ (Lisicon). *Electrochim. Acta* **1978**, *23*, 1395-1397.
- 31
32
33
34 (14) Hong H. Y. P. Crystal Structures and Crystal Chemistry in the System $\text{Na}_{1+x}\text{Zr}_2\text{Si}_x\text{P}_{3-x}\text{O}_{12}$. *Mater. Res. Bull.* **1976**, *11*, 173-182.
- 35
36
37
38 (15) Inaguma Y.; Liqun C.; Itoh M.; Nakamura T.; Uchida T.; Ikuta H.; Wakihara M. High Ionic Conductivity in Lithium Lanthanum Titanate. *Solid State Commun.* **1993**, *86*, 689-693.
- 39
40
41
42 (16) Thangadurai V.; Weppner W. $\text{Li}_6\text{Ala}_2\text{Ta}_2\text{O}_{12}$ (A = Sr, Ba): Novel Garnet-Like Oxides for Fast Lithium Ion Conduction. *Adv. Funct. Mater.* **2005**, *15*, 107-112.
- 43
44
45
46 (17) Hayashi A.; Minami K.; Tatsumisago M. Development of Sulfide Glass-Ceramic Electrolytes for All-Solid-State Lithium Rechargeable Batteries. *J. Solid State Electrochem.* **2010**, *14*, 1761-1767.
- 47
48
49
50 (18) Knauth P. Inorganic Solid Li Ion Conductors: An Overview. *Solid State Ionics* **2009**, *180*, 911-916.
- 51
52
53
54 (19) Aono H.; Sugimoto E.; Sadaoka Y.; Imanaka N.; Adachi G.-y. Dc Conductivity of $\text{Li}_{1.3}\text{Al}_{0.3}\text{Ti}_{1.7}(\text{PO}_4)_3$ Ceramic with Li Electrodes. *Chem. Lett.* **1991**, 1567-1570.
- 55
56
57
58
59
60

- 1
2
3
4 (20) Lee J. S.; Tai Kim S.; Cao R.; Choi N. S.; Liu M.; Lee K. T.; Cho J. Metal–Air Batteries with High
5 Energy Density: Li–Air Versus Zn–Air. *Adv. Eng. Mater.* **2011**, *1*, 34-50.
6
7
8 (21) Wang S.; Ding Y.; Zhou G.; Yu G.; Manthiram A. Durability of the $\text{Li}_{1.3}\text{Al}_{0.3}\text{Ti}_{1.7}(\text{PO}_4)_3$ Solid
9 Electrolyte in Lithium–Sulfur Batteries. *ACS Energy Lett.* **2016**, *1*, 1080-1085.
10
11
12 (22) Yu X.; Bi Z.; Zhao F.; Manthiram A. Polysulfide-Shuttle Control in Lithium-Sulfur Batteries with a
13 Chemically/Electrochemically Compatible Nasicon-Type Solid Electrolyte. *Adv. Eng. Mater.* **2016**,
14 *6*, 1601392-1601400.
15
16
17 (23) Ding F.; Xu W.; Shao Y.; Chen X.; Wang Z.; Gao F.; Liu X.; Zhang J.-G. H+ Diffusion and
18 Electrochemical Stability of $\text{Li}_{1+x}\text{Al}_x\text{Ti}_{2-x}\text{Si}_y\text{P}_{3-y}\text{O}_{12}$ Glass in Aqueous Li/Air Battery Electrolytes.
19 *J. Power Sources* **2012**, *214*, 292-297.
20
21
22 (24) Amiki Y.; Sagane F.; Yamamoto K.; Hirayama T.; Sudoh M.; Motoyama M.; Iriyama Y.
23 Electrochemical Properties of an All-Solid-State Lithium-Ion Battery with an in-Situ Formed
24 Electrode Material Grown from a Lithium Conductive Glass Ceramics Sheet. *J. Power Sources*
25 **2013**, *241*, 583-588.
26
27
28 (25) Yamamoto K.; Iriyama Y.; Asaka T.; Hirayama T.; Fujita H.; Nonaka K.; Miyahara K.; Sugita Y.;
29 Ogumi Z. Direct Observation of Lithium-Ion Movement around an in-Situ-Formed-Negative-
30 Electrode/Solid-State-Electrolyte Interface During Initial Charge–Discharge Reaction.
31 *Electrochem. Commun.* **2012**, *20*, 113-116.
32
33
34 (26) Aboulaich A.; Bouchet R.; Delaizir G.; Seznec V.; Tortet L.; Morcrette M.; Rozier P.; Tarascon J.-M.;
35 Viallet V.; Dollé M. A New Approach to Develop Safe All-Inorganic Monolithic Li-Ion Batteries.
36 *Adv. Eng. Mater.* **2011**, *1*, 179-183.
37
38
39 (27) Zhu Y.; He X.; Mo Y. Origin of Outstanding Stability in the Lithium Solid Electrolyte Materials:
40 Insights from Thermodynamic Analyses Based on First-Principles Calculations. *ACS Appl. Mater.*
41 *Interfaces* **2015**, *7*, 23685-23693.
42
43
44 (28) Hartmann P.; Leichtweiss T.; Busche M. R.; Schneider M.; Reich M.; Sann J.; Adelhelm P.; Janek J.
45 Degradation of Nasicon-Type Materials in Contact with Lithium Metal: Formation of Mixed
46 Conducting Interphases (MCI) on Solid Electrolytes. *J. Phys. Chem. C* **2013**, *117*, 21064-21074.
47
48
49 (29) Nairn K.; Best A.; Newman P.; MacFarlane D.; Forsyth M. Ceramic-Polymer Interface in
50 Composite Electrolytes of Lithium Aluminium Titanium Phosphate and Polyetherurethane
51 Polymer Electrolyte. *Solid State Ionics* **1999**, *121*, 115-119.
52
53
54
55
56
57
58
59
60

- 1
2
3 (30) Zhou W.; Wang S.; Li Y.; Xin S.; Manthiram A.; Goodenough J. B. Plating a Dendrite-Free Lithium
4 Anode with a Polymer/Ceramic/Polymer Sandwich Electrolyte. *JACS* **2016**, *138*, 9385-9388.
5
6
7 (31) Yue L.; Ma J.; Zhang J.; Zhao J.; Dong S.; Liu Z.; Cui G.; Chen L. All Solid-State Polymer Electrolytes
8 for High-Performance Lithium Ion Batteries. *Energy Storage Materials* **2016**, *5*, 139-164.
9
10
11 (32) Borghini M. C.; Mastragostino M.; Zanelli A. Investigation on Lithium/Polymer Electrolyte
12 Interface for High Performance Lithium Rechargeable Batteries. *J. Power Sources* **1997**, *68*, 52-
13 58.
14
15
16 (33) Appetecchi G. B.; Croce F.; Dautzenberg G.; Mastragostino M.; Ronci F.; Scrosati B.; Soavi F.;
17 Zanelli A.; Alessandrini F.; Prosini P. P. Composite Polymer Electrolytes with Improved Lithium
18 Metal Electrode Interfacial Properties: I. Electrochemical Properties of Dry PEO-LiX Systems. *J.*
19 *Electrochem. Soc.* **1998**, *145*, 4126-4132.
20
21
22 (34) Orsini F.; Du Pasquier A.; Beaudoin B.; Tarascon J. M.; Trentin M.; Langenhuizen N.; De Beer E.;
23 Notten P. In Situ Scanning Electron Microscopy (SEM) Observation of Interfaces within Plastic
24 Lithium Batteries. *J. Power Sources* **1998**, *76*, 19-29.
25
26
27 (35) Dudney N. J.; Neudecker B. J. Solid State Thin-Film Lithium Battery Systems. *Curr. Opin. Solid. St.*
28 *M.* **1999**, *4*, 479-482.
29
30
31 (36) Hasegawa S.; Imanishi N.; Zhang T.; Xie J.; Hirano A.; Takeda Y.; Yamamoto O. Study on
32 Lithium/Air Secondary Batteries-Stability of Nasicon-Type Lithium Ion Conducting Glass-
33 Ceramics with Water. *J. Power Sources* **2009**, *189*, 371-377.
34
35
36 (37) West W. C.; Whitacre J. F.; Lim J. R. Chemical Stability Enhancement of Lithium Conducting Solid
37 Electrolyte Plates Using Sputtered Lipon Thin Films. *J. Power Sources* **2004**, *126*, 134-138.
38
39
40 (38) Kozen A. C.; Lin C.-F.; Pearse A. J.; Schroeder M. A.; Han X.; Hu L.; Lee S.-B.; Rubloff G. W.; Noked
41 M. Next-Generation Lithium Metal Anode Engineering Via Atomic Layer Deposition. *ACS Nano*
42 **2015**, *9*, 5884-5892.
43
44
45 (39) Lin C. F.; Kozen A. C.; Noked M.; Liu C.; Rubloff G. W. ALD Protection of Li-Metal Anode Surfaces-
46 Quantifying and Preventing Chemical and Electrochemical Corrosion in Organic Solvent. *Adv.*
47 *Mater. Interfaces* **2016**, *3*, 1600426-1600433.
48
49
50 (40) Wang B.; Liu J.; Sun Q.; Li R.; Sham T. K.; Sun X. Atomic Layer Deposition of Lithium Phosphates
51 as Solid-State Electrolytes for All-Solid-State Microbatteries. *Nanotechnology* **2014**, *25*, 504007.
52
53
54
55
56
57
58
59
60

- 1
2
3 (41) Zhao Y.; Goncharova L. V.; Sun Q.; Li X.; Lushington A.; Wang B.; Li R.; Dai F.; Cai M.; Sun X.
4 Robust Metallic Lithium Anode Protection by the Molecular-Layer-Deposition Technique. *Small*
5 *Methods*. **2018**, 5, 1700417-1700425.
6
7
8 (42) Han X.; Gong Y.; Fu K. K.; He X.; Hitz G. T.; Dai J.; Pearse A.; Liu B.; Wang H.; Rubloff G. Negating
9 Interfacial Impedance in Garnet-Based Solid-State Li Metal Batteries. *Nat. Mater.* **2017**, 16, 572-
10 579.
11
12
13 (43) Luo W.; Gong Y.; Zhu Y.; Li Y.; Yao Y.; Zhang Y.; Fu K. K.; Pastel G.; Lin C. F.; Mo Y.; Wachsman E.
14 D.; Hu L. Reducing Interfacial Resistance between Garnet-Structured Solid-State Electrolyte and
15 Li-Metal Anode by a Germanium Layer. *Adv. Mater.* **2017**, 29, 1606042-1606049.
16
17
18 (44) Tsai C. L.; Roddatis V.; Chandran C. V.; Ma Q.; Uhlenbruck S.; Bram M.; Heitjans P.; Guillon O.
19 $\text{Li}_7\text{La}_3\text{Zr}_2\text{O}_{12}$ Interface Modification for Li Dendrite Prevention. *ACS Appl. Mater. Interfaces* **2016**,
20 8, 10617-10626.
21
22
23 (45) Zhao Y.; Goncharova L. V.; Lushington A.; Sun Q.; Yadegari H.; Wang B.; Xiao W.; Li R.; Sun X.
24 Superior Stable and Long Life Sodium Metal Anodes Achieved by Atomic Layer Deposition. *Adv.*
25 *Mater.* **2017**, 29, 1606663-1606670.
26
27
28 (46) Wang B.; Liu J.; Sun Q.; Li R.; Sham T.-K.; Sun X. Atomic Layer Deposition of Lithium Phosphates
29 as Solid-State Electrolytes for All-Solid-State Microbatteries. *Nanotechnology* **2014**, 25, 504007.
30
31
32 (47) Kobayashi K.; Yabashi M.; Takata Y.; Tokushima T.; Shin S.; Tamasaku K.; Miwa D.; Ishikawa T.;
33 Nohira H.; Hattori T.; Sugita Y.; Nakatsuka O.; Sakai A.; Zaima S. High Resolution-High Energy X-
34 Ray Photoelectron Spectroscopy Using Third-Generation Synchrotron Radiation Source, and Its
35 Application to Si-High K Insulator Systems. *Appl. Phys. Lett.* **2003**, 83, 1005-1007.
36
37
38 (48) Thiess S.; Kunz C.; Cowie B. C. C.; Lee T. L.; Renier M.; Zegenhagen J. Hard X-Ray Photoelectron
39 Spectroscopy from 5–14.5 Kev. *Solid State Commun.* **2004**, 132, 589-594.
40
41
42 (49) Liu J.; Wang B.; Sun Q.; Li R.; Sham T.-K.; Sun X. Atomic Layer Deposition of Hierarchical
43 CNTs@FePO₄ Architecture as A 3D Electrode for Lithium-Ion and Sodium-Ion Batteries. *Adv.*
44 *Mater. Interfaces* **2016**, 3, 1600468-n/a.
45
46
47 (50) Li X.; Lushington A.; Sun Q.; Xiao W.; Liu J.; Wang B.; Ye Y.; Nie K.; Hu Y.; Xiao Q.; Li R.; Guo J.;
48 Sham T.-K.; Sun X. Safe and Durable High-Temperature Lithium–Sulfur Batteries Via Molecular
49 Layer Deposited Coating. *Nano Lett.* **2016**, 16, 3545-3549.
50
51
52 (51) Tsai C. L.; Roddatis V.; Chandran C. V.; Ma Q.; Uhlenbruck S.; Bram M.; Heitjans P.; Guillon O.
53 $\text{Li}_7\text{La}_3\text{Zr}_2\text{O}_{12}$ Interface Modification for Li Dendrite Prevention. *ACS Appl. Mater. Interfaces* **2016**,
54 8, 10617-10626.
55
56
57
58
59
60

- 1
2
3
4 (52) Yamamoto K.; Iriyama Y.; Hirayama T. Visualization of Electrochemical Reactions in All-Solid-
5 State Li-Ion Batteries by Spatially Resolved Electron Energy-Loss Spectroscopy and Electron
6 Holography. *Mater. Trans.* **2015**, *56*, 617-624.
7
8
9 (53) Ohtomo A.; Muller D. A.; Grazul J. L.; Hwang H. Y. Artificial Charge-Modulation in Atomic-Scale
10 Perovskite Titanate Superlattices. *Nature* **2002**, *419*, 378-380.
11
12 (54) Koerver, R.; Zhang, W.; de Biasi, L.; Schweidler, S.; Kondrakov, A.; Kolling, S.; Brezesinski, T.;
13 Hartmann, P.; Zeier, W.; Janek, J. Chemo-mechanical Expansion of Lithium Electrode Materials—On the
14 Route to Mechanically Optimized All-Solid-State Batteries. *Energy Environ. Sci.* **2018**, *11*, 2142-2158
15
16 (55) Xin, S.; You, Y.; Wang, S.; Gao, H.C.; Yin, Y.X.; Guo, Y.G. Solid-state Lithium Metal Batteries
17 Promoted by Nanotechnology: Progress and Prospects. *ACS Energy Lett.*, **2017**, *2*, 1385-1394.
18
19
20
21
22
23
24
25
26
27
28
29
30
31
32
33
34
35
36
37
38
39
40
41
42
43
44
45
46
47
48
49
50
51
52
53
54
55
56
57
58
59
60

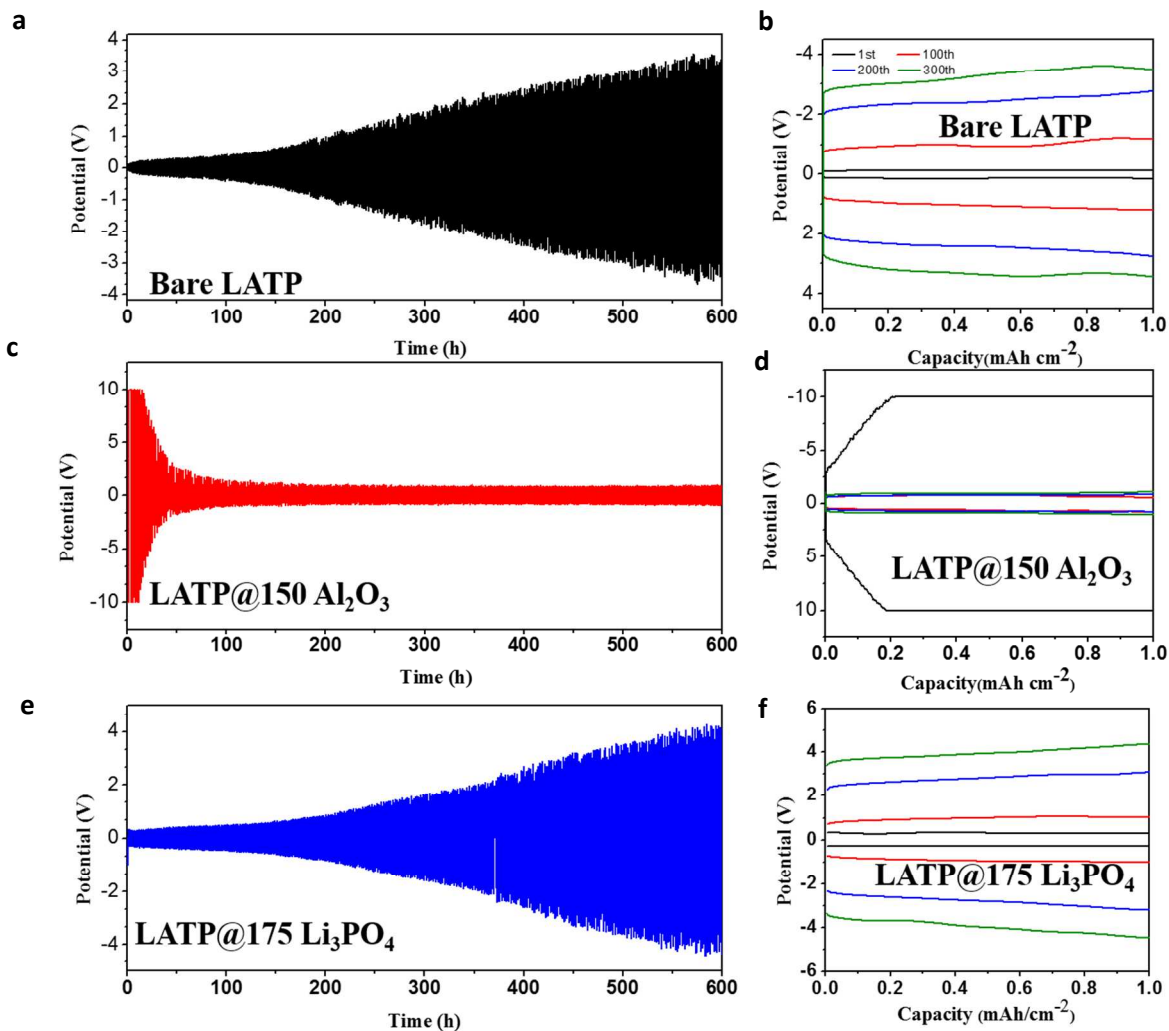


Figure 1: Electrochemical behavior of the LATP/Li symmetrical cell with and without interlayer coatings at a current density of 0.01 mA cm^{-2} . Each cycle take 2h for lithium stripping and plating; (a-b) Cycling behavior and voltage profile of bare LATP/Li at the 1st, 100th, 200th and 300th cycle; (c-d) Cycling behavior and voltage profile of LATP@150Al₂O₃/Li at the 1st, 100th, 200th and 300th cycle ;(e-f) Cycling behavior and voltage profile of LATP@175Li₃PO₄/Li at the 1st, 100th, 200th and 300th cycle.

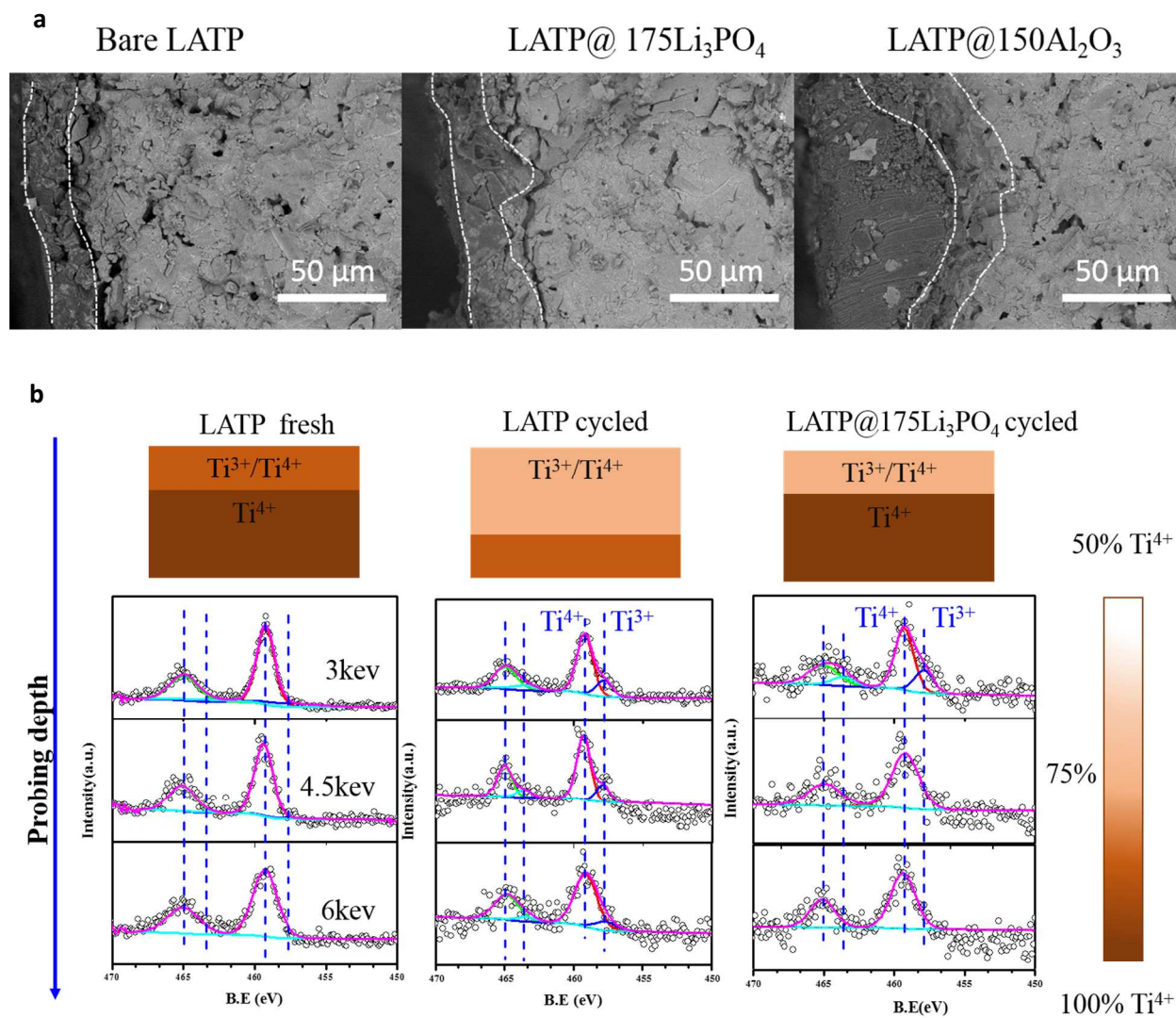


Figure 2. (a) Backscattering image of LATP pellets after 100 cycles. (b) HE-XPS of Ti 2p spectrum for pristine LATP, cycled-LATP and cycled-LATP@175 Li₃PO₄ for 100 cycles at different incident energy.

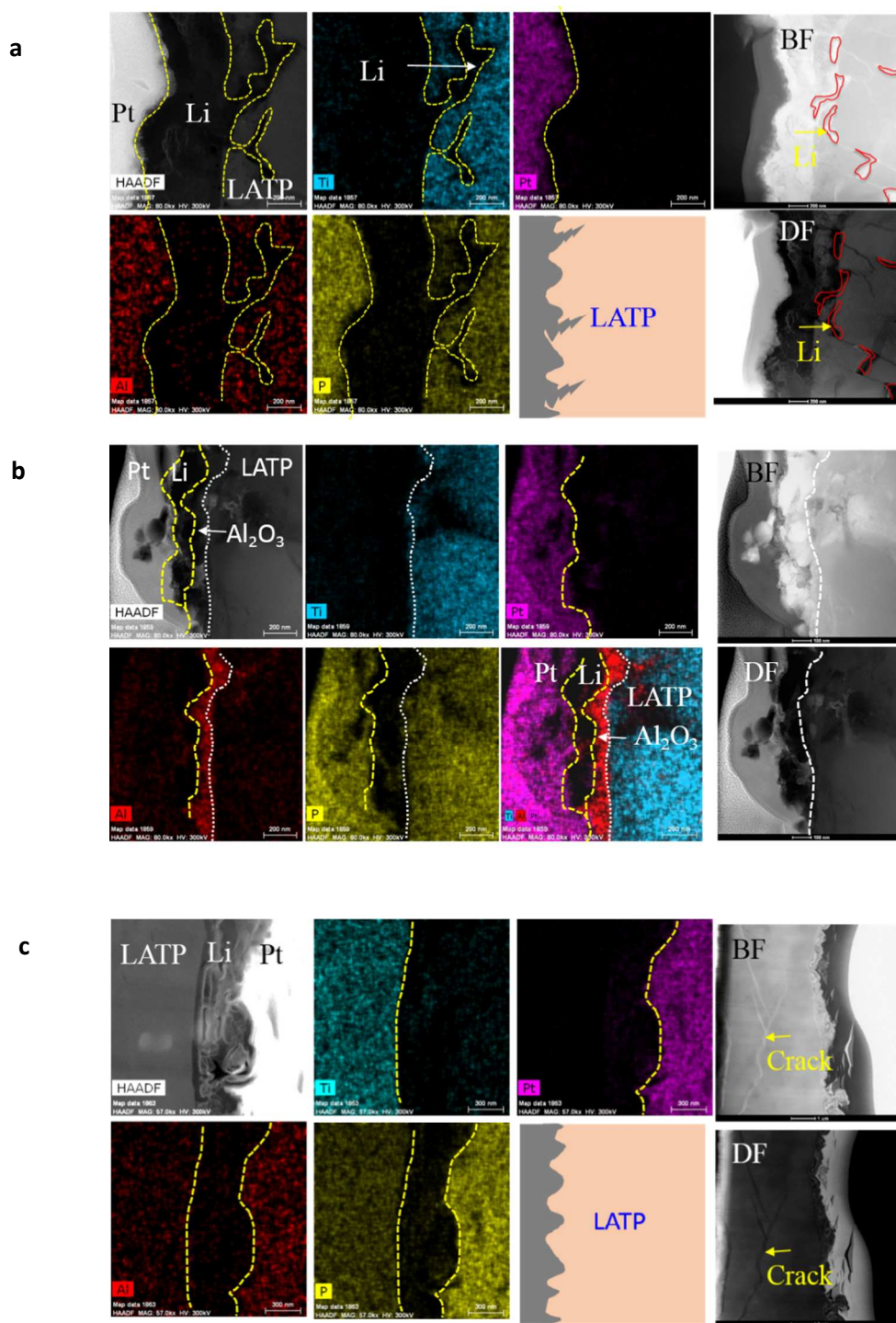
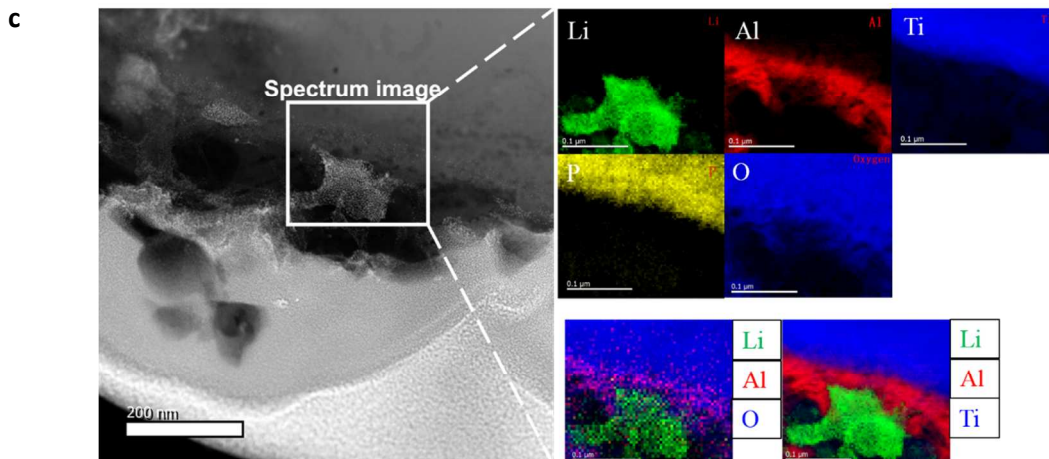
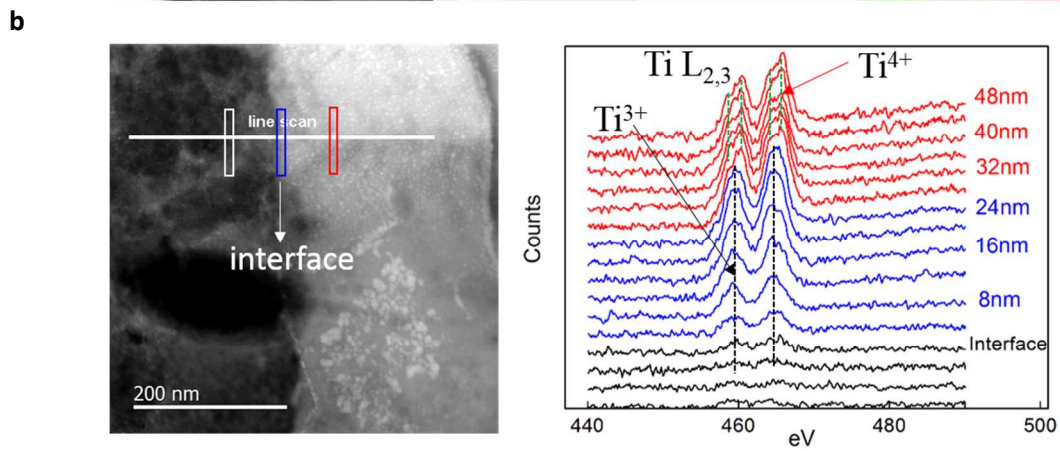
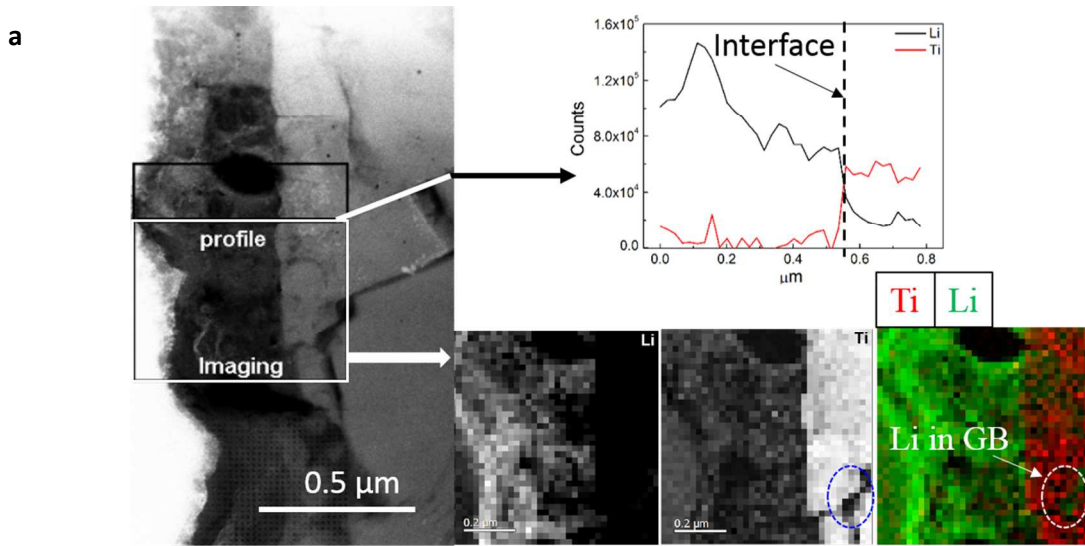
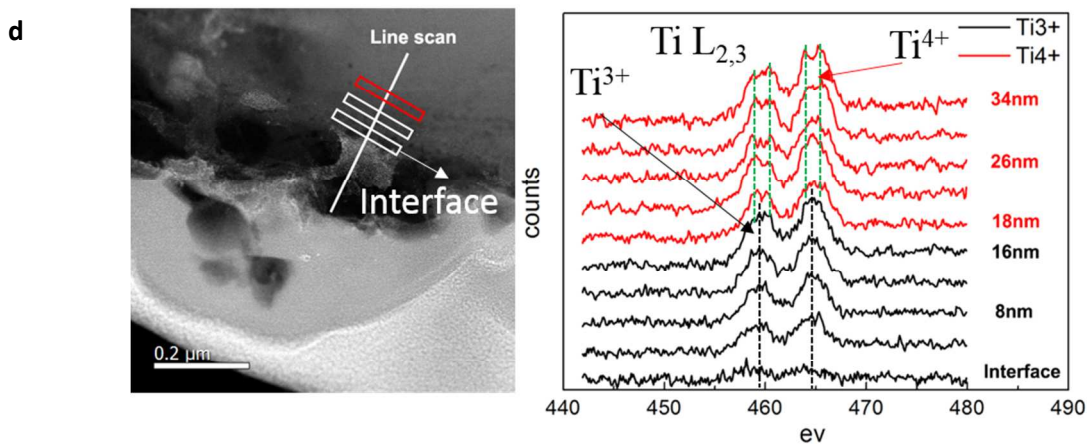
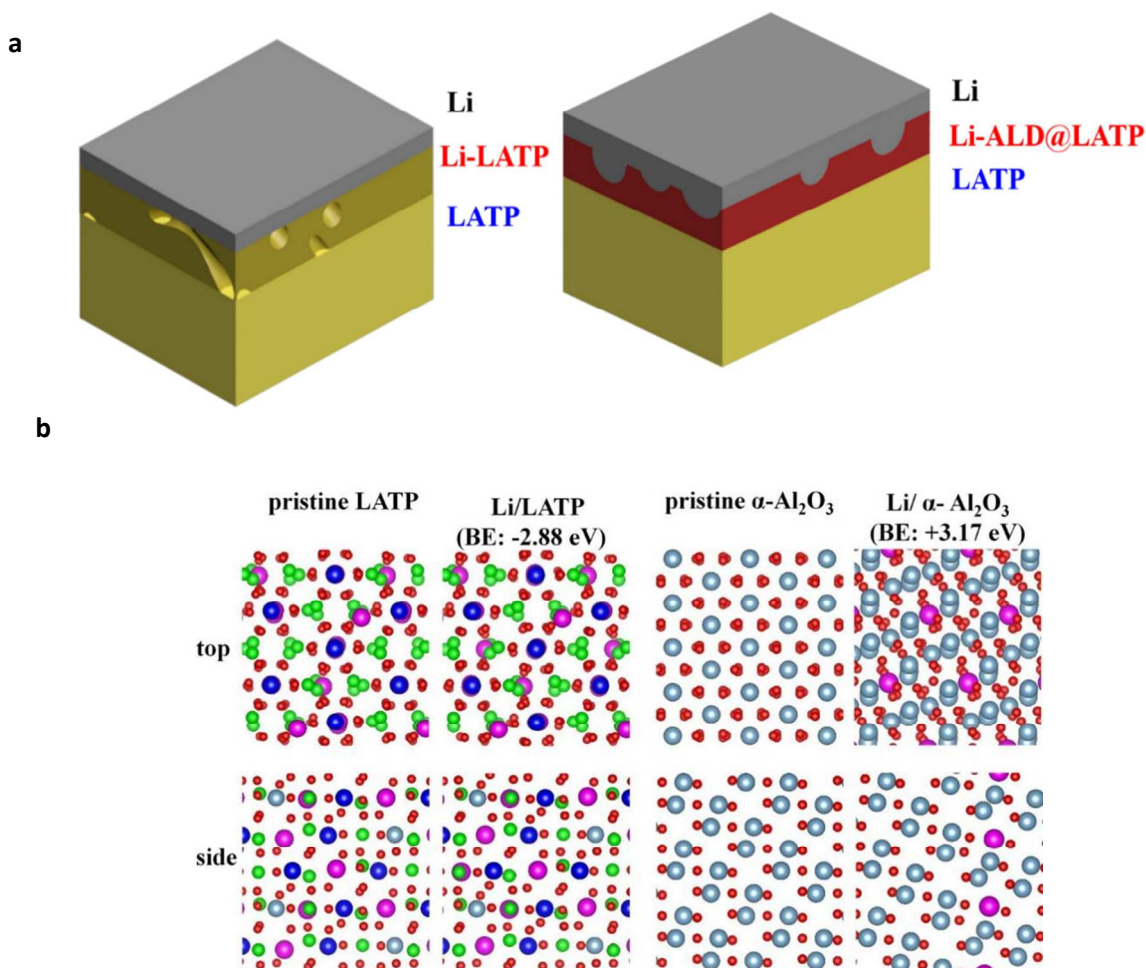


Figure 3. TEM-EDS mapping and BF (DF) images of the LATP pellet after 100 cycles. (a) Bare LATP, (b) LATP@150Al₂O₃, (c) LATP@175Li₃PO₄.





20 Figure 4. HRTEM-EELS of the LATP pellet after 100 cycles. (a-b) Element EELS mapping and Ti valence states in LATP interface;
 21 and Ti valence states in LATP interface;
 22 (c-d) Element EELS mapping and Ti valence states
 23 in LATP@150Al₂O₃ interface



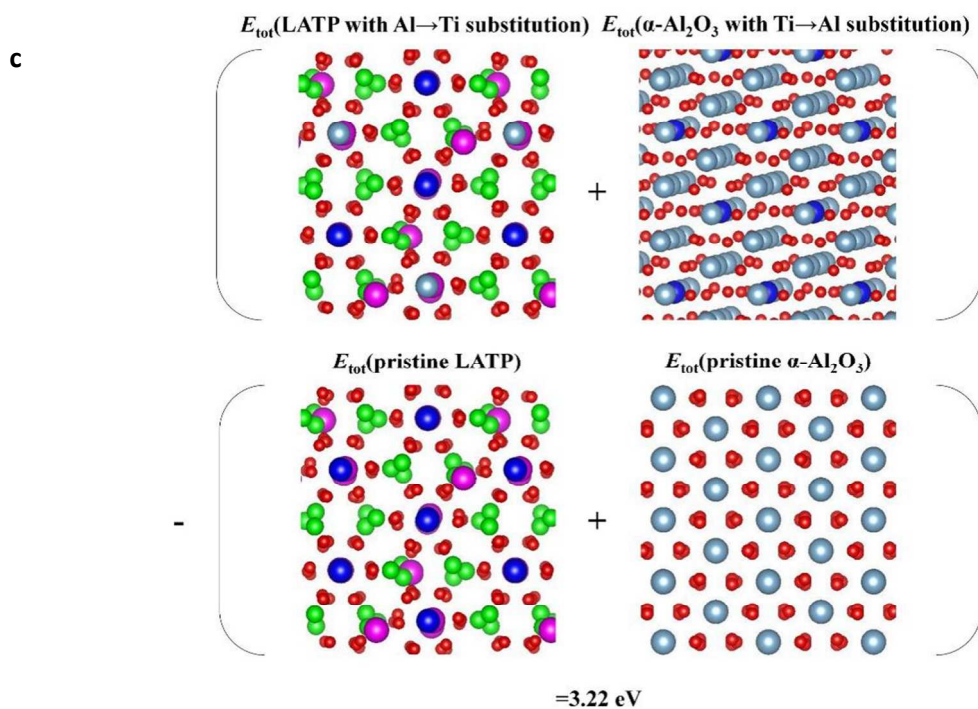
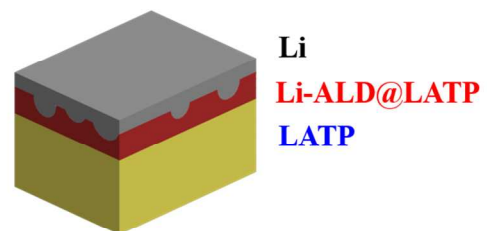
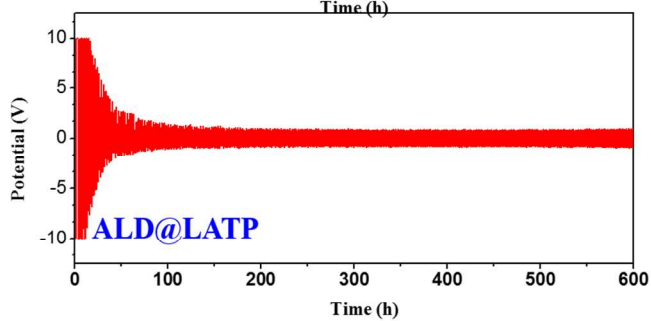
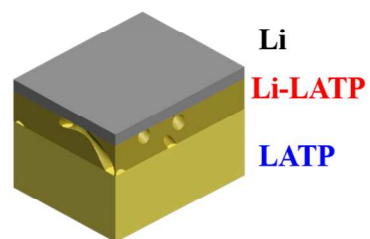
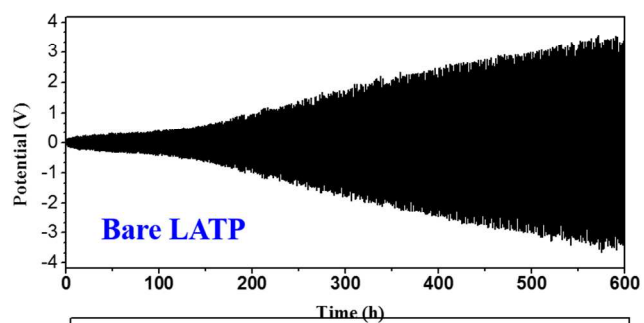


Figure 5. (a) Schematic diagram of LATP/Li interface with and without ALD Al_2O_3 , (b) Top and side views of bulk LATP and $\alpha\text{-Al}_2\text{O}_3$ structures with and without an extra Li. Calculated binding energy of a single Li into bulk systems is presented by BE. The BE values are referenced to bulk Li metal., (c) Schematic of the procedure to calculate the $\text{Al} \leftrightarrow \text{Ti}$ interchange energy between LATP and $\alpha\text{-Al}_2\text{O}_3$.



26
27
28
29
30
31
32
33
34
35
36
37
38
39
40
41
42
43
44
45
46
47
48
49
50
51
52
53
54
55
56
57
58
59
60

TOC Table of content